Solar Energy 163 443 (2018)

# Light trapping in ultrathin $CuIn_{1-x}Ga_xSe_2$ solar cells by dielectric nanoparticles

Guanchao Yin*,†,[a], Phillip Manley*,[a], Martina Schmid[a,b]

[a] Nanooptische Konzepte für die PV, Helmholtz-Zentrum Berlin für Materialien und Energie, Hahn-Meitner-Platz 1, 14109 Berlin, Germany

[b] Fakultät für Physik, Universität Duisburg-Essen & CENIDE, Lotharstraße 1, 47057 Duisburg, Germany

† **Corresponding author:** guanchao.yin@helmholtz-berlin.de

* Equal contribution

**Abstract**: In this work, light trapping effects based on dielectric nanoparticles (NPs) are numerically evaluated in ultrathin $CuIn_{1-x}Ga_xSe_2$ (CIGSe) solar cells for different locations of NPs, cell architectures and illumination directions, with relevant implications and optimized NP parameters being specified. The severe absorption in Mo is the main constraining factor for the effective implementation of light trapping NPs in ultrathin CIGSe cells. For a significant light absorption enhancement, it is favoured to integrate dielectric NPs at the back interface of CIGSe/back contact and employ transparent conductive oxide (TCO) back contacts rather than the conventional Mo. It is demonstrated, that under front illumination, the low-index (n = 1.5) hemispherical NPs at the CIGSe/TCO interface cause significant light trapping effects. The NP-patterned ultrathin cells achieve a maximum short circuit current density ($J_{sc}$) of 36.4 mA/cm$^2$ at an upper limit of 500 nm CIGSe thickness, which is as high as 94% $J_{sc}$ of their thick flat counterparts with a CIGSe thickness of 2000 nm. In contrast, under back illumination, the patterned ultrathin cells realize comparable absorption to the corresponding thick counterpart at a CIGSe thickness of only 300 nm and the maximum $J_{sc}$ (35.2 mA/cm$^2$) saturates at a CIGSe thickness of 425 nm. Further, $J_{sc}$ is less attenuated by the parasitic absorption in Al:ZnO (AZO) under back illumination than under front illumination in module configuration, where a much thicker AZO is required. This suggests that patterned ultrathin CIGSe solar cells under back illumination will be a promising cell architecture simultaneously for high efficiencies and less material usage in industrial module production.

**Keywords:** ultrathin $CuIn_{1-x}Ga_xSe_2$ solar cells, dielectric nanoparticles, light trapping, waveguide modes, back illumination, preferential scattering

# 1. Introduction

Photovoltaics, which convert sunlight to electricity, are a promising technology to address the environmental problems arising from burning fossil fuels by providing renewable and clean energy. Compared to the conventional bulk crystalline Si solar cells in the market, thin-film solar cells hold the promise to be more competitive, because they allow the reduction of material consumption and resulting manufacturing cost as well as improved flexibility in roll-to-roll manufacturing on bendable substrates. Among various thin-film solar cell technologies, $CuIn_{1-x}Ga_xSe_2$ (CIGSe) solar cells are unique for their high record efficiencies of 22.6% [1]. Furthermore, CIGSe solar cells offer a remarkably short energy payback time and a great tolerance towards environmental influences like shading and illumination intensity variations [2]. Despite these achievements and advantages, further cost reduction is desirable for driving mass production and large-scale deployment of CIGSe solar cells. Presently, the raw materials induced cost accounts for 50% of the module production [2] and In scarcity is likely to be a bottleneck when envisaging mass production [3,4]. To address the problems, one key approach is to thinning the CIGSe photoactive layers from typical 2-3 μm to below 500 nm. However, this will cause incomplete absorption, giving rise to a significantly reduced short circuit current density (a loss of more than 6 $mA/cm^2$ in $J_{sc}$,) and poor cell performance [5–8]. Therefore, light trapping is crucial to maintain high efficiencies of ultrathin CIGSe cells (with a sub-500 nm absorber thickness).

Metallic nanoparticles (NPs) have been extensively explored for absorption enhancement in various types of solar cells, because they are able to exhibit plasmonic resonances allowing large-angular scattering and strong near-fields [9–13]. Yet, plasmonic NPs suffer from intrinsic parasitic absorption, limiting their potential for maximum absorption enhancement in photovoltaic devices [13-15]. More critically, plasmonic materials (*e.g.* Ag, Au) are not thermally compatible with the high-temperature CIGSe fabrication [16].

In recent years, wavelength-scale dielectric NPs have also gained tremendous attention in light trapping due to their strong scattering ability (relative to metallic ones) while being absorption free [17-20]. Furthermore, inorganic dielectric materials (*e.g.* $SiO_2$, $Al_2O_3$) are thermally stable, permits their experimental integration into CIGSe cells. Additionally, certain dielectric materials

were proved to contain intrinsic charges which can electrically benefit solar cells [21-23]. These distinctive features favour dielectric NPs as a light trapping tool for ultrathin CIGSe cells.

Compared to the intensive investigation in Si-based solar cells, the application of dielectric NPs to CIGSe solar cells for absorption enhancement is just emerging [24-28]. Though initial work has realized absorption enhancement to varied success, no systematic research has been performed to identify how to effectively implement light trapping NPs in ultrathin CIGSe solar cells. Plus, CIGSe solar cells have a distinctively different cell architecture and opto-electronic properties from Si-based cells. Those suggest that the effective implementation of light trapping NPs in ultrathin CIGSe solar cells may not be easily generalized from similar technologies.

In this contribution, we start from analyzing optical losses in ultrathin CIGSe solar cells. To identify the potential of NPs in ultrathin CIGSe solar cells from the perspective of absorption enhancement, light trapping effects of dielectric hemispheres for different locations of NPs, cell architectures, illumination directions, are comprehensively evaluated with relevant implications and optimized NP parameters being specified.

# 2. Simulation

The theoretical CIGSe solar cell model is based on our lab-scale architectures with a typical structure of Al:ZnO(AZO)/ZnO/CdS/CIGSe/back contact/substrate from top to bottom. For the window and buffer layers (AZO/ZnO/CdS), the thicknesses are 240/130/50 nm. The back contact is Mo or alternatively Sn:$In_2O_3$ (ITO) with a thickness of 200 nm and a sheet resistance < 10 Ω/sq. The CIGSe layer here corresponds to a Ga/[Ga+In] ratio of 0.35 and a minimum bandgap of 1.05 eV. The input optical constants (refractive index *n*, extinction coefficient *k*) of each individual layer (except Mo) are extracted by transfer-matrix method [29]. Mo data was obtained using spectroscopic ellipsometry.

For optical simulations on flat CIGSe solar cells, an analytical program based on transfer-matrix method (RefDex) is used [30]. To understand the optical influences of NPs on ultrathin CIGSe solar cells, we perform finite element method (FEM) simulations using the software package JCMsuite [31]. In all optical simulations, interface roughness is not taken into account, but we don't expect that the overall trend will be substantially influenced since the interface roughness is typically low in experimental samples. For overall comparison, reflection (*R*), absorption (*Abs*) and transmission (*T*) are converted into current density *J*, assuming the complete conversion

under standard AM 1.5 solar irradiation. The current density out of absorption in the CIGSe layer ($Abs_{CIGSe}$) is specially referred to as short circuit current density $J_{sc}$.

# 3. Identification of optical losses

Table 1 Cell structures for identifying optical losses in ultrathin CIGSe solar cells

| No. | Structure (from top to bottom) | $d_{CIGSe}$ (nm) |
|---|---|---|
| **N1** | AZO/ZnO/CdS/CIGSe/**Mo**/glass substrate | 2000 (thick) |
| **N2** | AZO/ZnO/CdS/CIGSe/**Mo**/glass substrate | 400 (ultrathin) |
| **N3** | AZO/ZnO/CdS/CIGSe/**Ag**/glass substrate | 400 |
| **N4** | AZO/ZnO/CdS/CIGSe/**ITO/glass substrate/Ag mirror** | 400 |

To identify optical losses in ultra-thin CIGSe solar cells, we start from the simulations of flat devices and compare optical responses (*R*/*T*/*Abs*) of cells in varied absorber thicknesses ($d_{CIGSe}$) as well as different back contacts. The detailed cell structures are listed in Table 1.

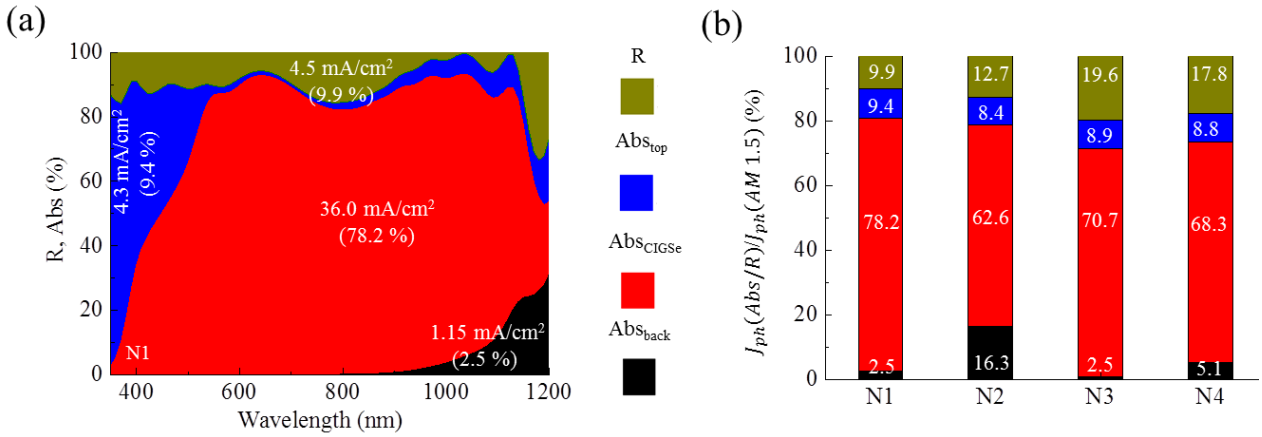


Figure 1(a) Optical responses (*R*/*T*/*Abs*) of thick CIGSe solar cells at $d_{CIGSe}$ = 2000 nm (N1), (b) weights of each individual response $\frac{J(Abs/R/T)}{J(AM\ 1.5)}$ of cell architectures in Table 1.

Amongst all the layers in CIGSe solar cell devices, only the absorption in the CIGSe absorber layer ($Abs_{CIGSe}$) contributes to the effective photocurrent, *R*, *T* and *Abs* in other layers are lost. We start from thick cells on a conventional Mo back contact at $d_{CIGSe}$ = 2000 nm (N1) and its optical responses (*R*/*T*/*Abs*) are plotted in Figure 1(a). The weights of *R*/*T*/*Abs* are also labelled in terms

of $\frac{J(Abs/R/T)}{J(AM\ 1.5)}$ in Figure 1(a). It can be observed that $Abs_{CIGSe}$ dominates the spectrum of interest and the optical losses are sub-divided into 3 sections: *R*, *Abs* in AZO/ZnO/CdS ($Abs_{top}$) and back contact ($Abs_{back}$). *R* loss covers the whole spectrum of interest. The parasitic $Abs_{top}$ dominates the absorption in the visible range (<550 nm) due to inter-band absorption of AZO/ZnO/CdS. As to $Abs_{top}$ in the long wavelength range, this is related to free carrier-induced absorption in AZO. Since AZO/ZnO/CdS layers are on top of the CIGSe layer, $Abs_{top}$ is inevitable. The parasitic $Abs_{back}$ starts from the wavelength where light is not completely absorbed by the CIGSe layer and is negligible for thick cells.

For comparison, $\frac{J(Abs/R/T)}{J(AM\ 1.5)}$ shares for $d_{CIGSe}$ = 400 nm (N2) are studied and listed in Figure 1(b). As observed, the ultrathin cells feature increased $Abs_{back}$ and *R* at a cost of a dramatic drop in $Abs_{CIGSe}$, and $Abs_{back}$ is becoming the main optical loss. It accounts for a share of 16.3%, whereas the corresponding value in the thick cells (N1) is only 2.5%. This can be interpreted due to the poor reflective ability of Mo: light reaching Mo will be mainly absorbed by Mo rather than being reflected back into CIGSe [32, 33]. As the CIGSe thickness reduces, more light hits Mo and the parasitic absorption in Mo thereby increases. For the increase in *R*, this is related to the increased intensity of light escaping ultrathin solar cells out of incomplete absorption, which mainly lies in the infrared range.

The ratios, $\frac{J(Abs/R/T)}{J(AM\ 1.5)}$ for ultrathin cells on Ag back contact with nearly perfect rear reflectivity (N3) are also shown in Figure 1(b). The parasitic $Abs_{back}$ reduces to a negligible level and the share $Abs_{CIGSe}$ accounts for significantly enhances from 62.6% to 70.7 % compared to the cell on Mo (N2), despite of being still lower than the value of thick cells N1. Unfortunately, the direct implementation of metallic materials (Ag, Al, Au) having much better reflectivity as back contact is not experimentally feasible due to their thermal incompatibility with high-temperature CIGSe fabrication. Lifting off and transferring solar cells from Mo onto Au back contact for improving interface reflectivity has been experimentally realized [34]. However, the lift-off process is applicable to the size of a few $cm^2$ and the absorption enhancement is limited by only a double optical path. An alternative back contact, which is experimentally feasible and exhibits low absorption ability, are the transparent conductive oxides (TCOs) [35-37]. Their back interface reflectivity is also poor, which can however be overcome by a reflector at the rear side of the

glass substrate. $\frac{J(Abs/R/T)}{J(AM\ 1.5)}$ fractions for ultrathin cells on ITO/glass/Ag back reflector (N4) are listed in Figure 1(b) as well. The parasitic $Abs_{back}$ (both ITO and Ag mirror) takes a small portion of 5.1% and is greatly lower than 16.3% in the case of Mo back contact. As a result, the $Abs_{CIGSe}$ fraction improves to 68.3%, which is nearly 6% higher than the value on Mo (N2).

In conclusion, the parasitic $Abs_{back}$ is the main optical loss for ultrathin cells on Mo back contact. This indicates that, in order to obtain a comparable $Abs_{CIGSe}$ to their thick counterparts, ultrathin CIGSe solar cells should reduce light intensity reaching Mo into a negligible level, otherwise a dramatic $Abs_{back}$ is inevitable. Whereas for ITO/glass/Ag mirror back contact, ultrathin cells allows light hitting back contact in multiple passes, which mitigates the requirements for light trapping NPs. It should be noted here that CIGSe solar cells normally exhibit inferior electrical performance on TCO than on Mo due to the mismatch of work function between CIGSe and TCO. However, recent reports have shown that inserting a few nm thick hole transporting layer can address this problem, holding the promise to utilize the advantages of TCO back contacts [38, 39].

# 4. Light trapping NPs on top

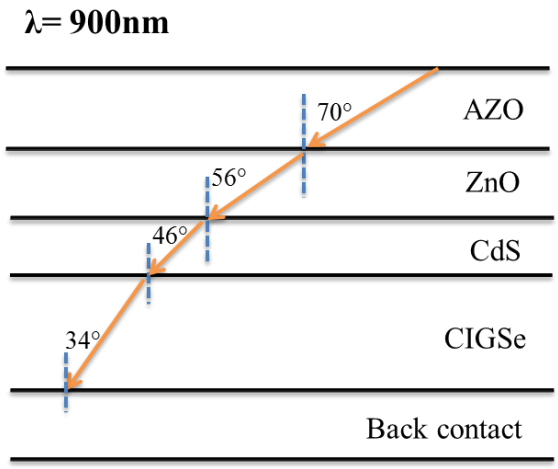


Figure 2 Sketch of angle shrinkage of light (λ = 900 nm) scattered from top: Based on Snell's law, the refractive indices gradually increasing from AZO to CIGSe reduce the scattering angle of 70° (in AZO) to 34° (in CIGSe).

For the stability consideration of electrical properties in photovoltaic devices, light trapping NPs are typically placed out of the p-n junction and in many cases on top of the cells. Light trapping

effects from the top can be generally decomposed into improved coupling (*R* reduction) and large angular scattering. However, previous studies of light trapping nanostructures on top of CIGSe solar cells (*e.g.* closely packed low-index $SiO_2$ nanospheres [24] and high-index $TiO_2$ nanopatterns [25] and textured AZO [40]), have ended with a modest $J_{sc}$ enhancement, showing the optimum light trapping effect comparable to the anti-reflection effect from a conventional $MgF_2$ layer. The underlying reasons are related to the specific cell architecture of CIGSe. On top of the photoactive CIGSe layer, there are three top layers (AZO/ZnO/CdS). According to Snell's law, scattering will suffer an angular shrinkage due to the continuously increasing refractive indices from AZO to CIGSe, which thus constrains the optical path enhancement in the CIGSe layer. For example at $\lambda$ = 900 nm, as shown in Figure 2, a scattering angle as high as 70° in AZO shrinks sharply to 34° in CIGSe. This corresponds to an optical path of only $1.2d_{CIGSe}$ in a single propagation and is much shorter than the absorption length at $\lambda$ = 900 nm. Further, AZO/ZnO/CdS layers exhibit broadband parasitic absorption (see Figure 1(a)), light passing through AZO/ZnO/CdS layers prior to the CIGSe absorber will attenuate the benefit of improved coupling as a result of a prior increase in $Abs_{top}$, which is aggravated by the prolonged optical path arising from angular scattering. This issue is particularly severe for cells on Mo back contact: on the one hand large angular scattering is required for a significant $Abs_{CIGSe}$ enhancement in a single pass, this will on the other hand induce an increase in $Abs_{top}$ and *R*, thus constrains or even worsens $Abs_{CIGSe}$.

Another disadvantage for light trapping NPs on top is, since light is propagating from a low-index material (AZO) to a high-index medium (CIGSe), scattering angles in CIGSe can not be beyond the critical angles and thus the possibility to trap light in CIGSe is lost. Combined with the above-mentioned attenuation points of light trapping effects from top, obtaining a significant $Abs_{CIGSe}$ enhancement and achieving a comparable $Abs_{CIGSe}$ to thick CIGSe cells is quite challenging for ultrathin cells with NPs on top.

# 5. Light trapping NPs at CIGSe/back contact

### 5.1 Front illumination

Placing light trapping NPs at interfaces touching absorbers allows light trapping effects to be directly utilized by CIGSe absorbers and avoid the attenuation effects from the top layers, similar phenomenon was also observed in Si solar cells [41]. Compared to the critical p-n junction

interface at CdS/CIGSe, it is electrically favourable to place light trapping NPs at CIGSe/back contact. 3D FEM simulations using JCMwave are performed to study optical behavior of hemispherical NPs in ultrathin CIGSe solar cells. Figure 3(a) shows the sketch of patterned CIGSe solar cells with NPs at CIGSe/back contact interface under front illumination. An anti-reflection $MgF_2$ layer with a thickness of 110 nm is added on top to reduce the Fabry–Pérot interferences. In the FEM simulation, a hexagonal computational domain with three sets of periodic boundary conditions in the *x*-*y* plane and perfectly matched layer (PML) boundary conditions in the *z* direction are used. A plane wave source is used incident antiparallel to the z axis, in order to simulate light incident from above the solar cell. To be comparable to the experimental morphology, the normal growth [42] of layers over NPs is assumed considering the NP incurred deformation of layers on top and the volume of individual layer is adjusted equally to the corresponding volume in the configuration of the flat reference. The shape of dielectric NPs is confined to represent a hemisphere, since we also studied other commonly used shapes like cylinder, conical frustrum and sphere and they exhibited comparable light absorption enhancement. They are in a hexagonal order with a radius of *r* and an edge-to-edge distance *l* as shown in Figure 3(b). To calculate the absorption in the layers of solar cells, the total field volume integration inside these individual layers is used. The unit simulation mesh structure is shown in supporting Figure S1.The index of NPs is set to 1.5, which is comparable to the thermally stable $SiO_2$ and $Al_2O_3$ and exhibits large index-contrast to CIGSe absorbers (~2.8). The optical constants for the individual layers of a CIGSe solar cell are plotted in Supporting Figure S2.

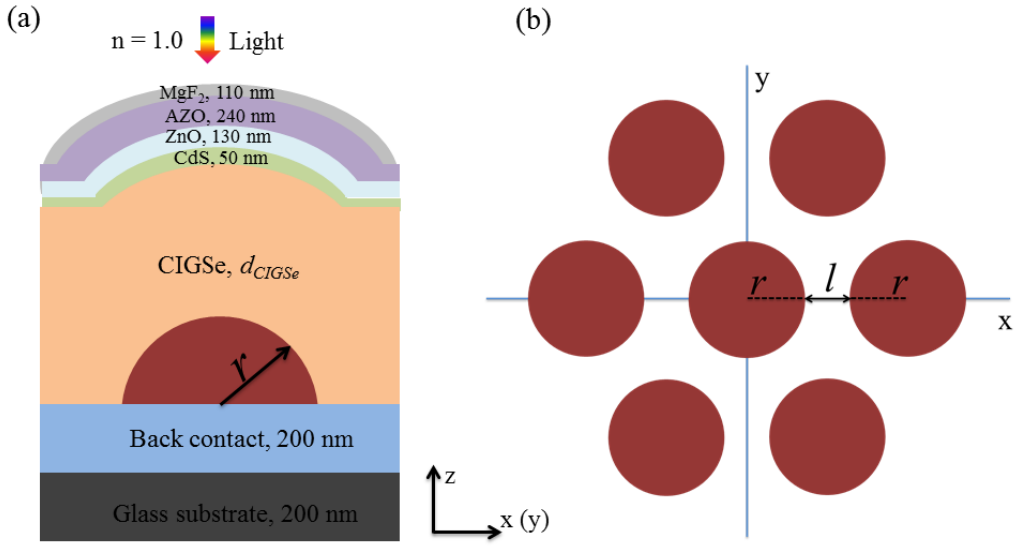

Figure 3(a) Sketch of hemisphere-patterned CIGSe solar cells under front illumination: the hemispheres are located at CIGSe/back contact interface, the layers on top of the hemisphere have a conformal growth. (b) Top view of the hexagonally arrayed hemispheres at the interface of CIGSe/back contact with a radius *r* and an edge-to-edge distance *l*.

We start from ultrathin cells on the conventional Mo back contact and Figure 4(a) compares *R/Abs* of NP-patterned solar cells (solid lines) to their flat counterparts (without NPs, dashed lines) at $d_{CIGSe}$ = 400 nm and (*r*, *l*) = (275, 75) nm. The (*r*, *l*) geometry parameter is within the optimum geometry range, which will be shown later. For flat cells, $Abs_{CIGSe}$ (red dashed line) reaches a maximum value of 95% at 550 nm and then incomplete absorption leads to a drop in $Abs_{CIGSe}$ for longer wavelengths. Remarkably, the patterned cell shows a pronounced $Abs_{CIGSe}$ enhancement (red dashed to red solid line) in the poor absorbing wavelengths, yielding a $J_{sc}$ enhancement of 3.2 mA/cm$^2$. This is mainly as a result of $Abs_{Mo}$ reduction (green dashed to green solid line). Furthermore, the *R* spectrum overall reduces after patterning and also contributes to the $Abs_{CIGSe}$ enhancement. $Abs_{top}$ does not significantly change upon the patterning and is not shown here.

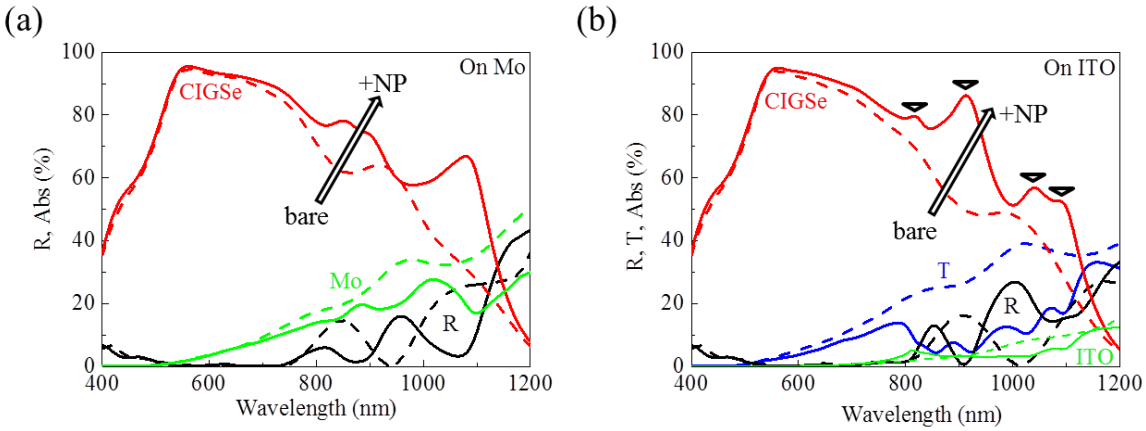


Figure 4 Optical responses (*R/Abs*) between flat (dashed lines) and patterned (solid lines) CIGSe solar cells (a) on Mo and (b) on ITO at $d_{CIGSe}$ = 400 nm and (*r*, *l*) = (275, 75) nm under front illumination

Even the major optical loss $Abs_{Mo}$ is substantially reduced after patterning, the remaining loss (green solid, 5.3 mA/cm$^2$) is still severe, which limits further $Abs_{CIGSe}$ enhancement. Actually, it is quite challenging to completely eliminate $Abs_{Mo}$ even by optimizing geometries of NPs, the reasons will be mentioned later. As stated above, TCO back contacts exhibit less absorption ability and thus render the potential of a lower $Abs_{back}$. For comparison, Figure 4(b) shows the plot of *R/T/Abs* between flat and patterned cells on ITO back contact. For flat cells, $Abs_{ITO}$ (green

dashed, Figure 4(b)) is around 10%, whereas $Abs_{Mo}$ (green dashed, Figure 4(a)) shows up to 30% beyond 900 nm in wavelength. $T$ (blue dashed) is becoming the main optical loss and shows up from the wavelength around 500 nm where incomplete absorption starts and is significantly increasing as the wavelength goes up. With the addition of NPs, similar to the case on Mo, cells on ITO exhibit a great $Abs_{CIGSe}$ enhancement (3.6 mA/cm$^2$) with a concomitant decrease in $T$ from 8.0 to 3.9 mA/cm$^2$ and in $Abs_{ITO}$ from 1.3 to 1.1 mA/cm$^2$. Overall, NP patterning gives a nearly equal $Abs_{CIGSe}$ between cells on ITO and on Mo. However, the remaining $T$ (3.9 mA/cm$^2$) for the patterned cells on ITO can be further utilized to a great extent by a reflector (*e.g.* Ag film, $TiO_2$ paste) at the rear side of glass substrate, which indicates that solar cells on ITO hold the potential to have a higher $Abs_{CIGSe}$. Due to this, we will limit the following investigations to cells on ITO.

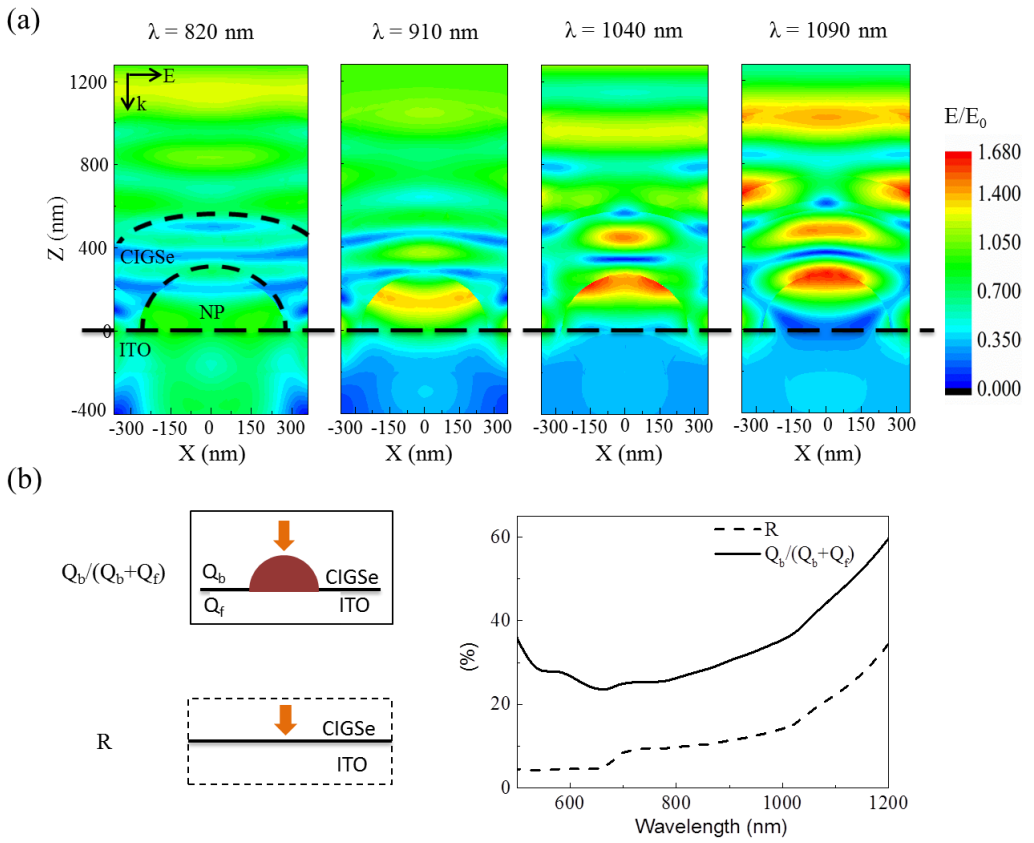


Figure 5(a) Near field distributions of patterned CIGSe solar cells on ITO at λ = 820, 910, 1040, 1090 nm, (b) comparison of interface reflectivity and backward scattering efficiency ($Q_b/(Q_b+Q_f)$) of a single NP at a CIGSe/ITO interface. Absorption ability for both CIGSe and ITO is turned off for the calculation in order to obtain the far field scattering, $Q_b$ and $Q_f$ are the normalized backward and forward cross sections, respectively.

We note that there are four pronounced $Abs_{CIGSe}$ enhancement peaks (λ = 820, 910, 1040, 1090 nm) for the patterned cells as the arrows indicate in Figure 4(b). A batch of simulations are done by tuning the edge-to-edge distance $l$ from 25 nm to 75 nm and the four resonance peaks are characterized by the linear red-shift in wavelength as $l$ (or pitch, $2r+l$) is enlarged (See supporting Figure S3). This suggests that diffraction from the NP array excites waveguide modes [43] which confines light within CIGSe absorbers and enhances $Abs_{CIGSe}$. The corresponding near field distributions are shown in Figure 5(a). The near field profiles are characteristic of regions of constructive and destructive interferences. At a free-space wavelength of 820 nm, where the bare CIGS absorption is still relatively strong, the peak field strength in the CIGSe absorber is only comparable to the incident light $E_0$. However, at the other three peaks, significant field confinements (higher than $E_0$) are present on the top part of hemispheres and within the absorber, which are located away from the ITO substrate. This visually explains the reduction of $Abs_{ITO}$ and $T$ after patterning as shown in Figure 4(b). Since the waveguide modes lie in the poor-absorbing range, the influence on the $Abs_{CIGSe}$ enhancement is substantial.

Besides the waveguide modes, the NPs are able to improve the CIGSe/ITO interface reflectivity, which arises from the backward scattering of NPs and contributes to $Abs_{CIGSe}$ enhancement as well. To investigate scattering behavior of a single hemisphere at CIGSe/ITO interface, all outer boundaries are set to PML. The forward and backward scattering behavior is calculated and normalized to the geometric cross section of a single hemisphere, and expressed in forward ($Q_f$) and backward ($Q_b$) scattering cross sections. The backward scattering efficiency (= $Q_b/(Q_b+Q_f)$) is compared to the bare CIGSe/ITO interface reflectivity in Figure 5(b). The extinction coefficient is neglected in both CIGSe and ITO for the calculation. We observe that the bare CIGSe/ITO reflectivity (dashed line) is quite low with a value under 20% in most of the spectral range, whereas a single NP exhibits a backward scattering efficiency (solid line) around 10% higher than the bare CIGSe/ITO reflectivity for all wavelengths. This indicates that the NPs are able to improve the CIGSe/ITO reflectivity and directly explains the broadband $Abs_{CIGSe}$ enhancement in the wavelength range from 550 to 800 nm, where waveguide modes are absent. It should be stressed that dielectric NPs with sizes comparable to or above the incident wavelength λ scatter light preferentially towards the incident wave propagation direction (forward scattering) [44-46]. In the case of front illumination, this indicates that light will be preferentially scattered into ITO. Nevertheless, compared to the bare interface, the presence of NPs enhances the backward scattering efficiency (towards CIGSe), which ($Q_b/(Q_b+Q_f)$) however still remains less

than 50% in most of the spectral range. This is unlike plasmonic metallic NPs, which are expected to dominantly scatter light into the high index medium of CIGSe (a greater refractive index of CIGSe than ITO). This is due to the larger number of multipole resonances present in dielectric NPs compared to metallic ones [15]. It also implies, in the case of Mo back contact in Figure 5(a), $Abs_{back}$ couldn't be eliminated to a marginal level and $Abs_{CIGSe}$ is thus suppressed. To clarify that the $Abs_{CIGSe}$ enhancement in the wavelength range of 550 to 800 nm is not arising from the modulation of Fabry–Pérot interferences due to the NP incurred $d_{CIGSe}$ change, the simulation is re-done assuming the NPs to be CIGSe but neglecting the extinction coefficient. Since NPs have the same refractive index as CIGSe absorbers, little light trapping effect from NPs is expected (Supporting Figure S4).

In order to evaluate the influence of the geometry ($r$, $l$) of hemisphere arrays on the $Abs_{CIGSe}$ enhancement, we map in Figure 6 integrated $J_{sc}$ as a function of ($r$, $l$) for $d_{CIGSe}$ = 400 nm. $r$ ranges from 200 to 300 nm and $l$ from 25 to 100 nm in steps of 25 nm. Notably, an apparent $Abs_{CIGSe}$ enhancement is demonstrated in the whole investigated geometry range (29.2 mA/cm$^2$ for the flat reference), with a maximum $J_{sc}$ of 33.0 mA/cm$^2$ achieved at ($r$, $l$) = (275, 75) nm. The broad geometry coverage can be correlated to the joint benefits of the broadband improvement of interface reflectivity and especially the multiplicity of waveguide modes covering the poor-absorbing wavelength range. From the fabrication perspective, the broad geometrical parameters of NPs represent a strong advantage inasmuch as the fabrication constraints are relaxed.

We arbitrarily define the optimum $J_{sc}$ values in the range from 32.8 to 33.0 mA/cm$^2$. Another feature in Figure 6 is that the optimum geometry region follows an overall trend of an increasing $l$ coupled with a decreasing $r$. Since the pitch is the summation of $l$ and twice $r$, increasing one while decreasing the other will tend to leave the pitch constant, and thus the wavelength positions of waveguide modes in the optimum range, which confirms the above-mentioned statement of substantial influence of waveguide modes on the $J_{sc}$ enhancement. This also suggests that the optimum ($r$, $l$) range for $d_{CIGSe}$ = 400 nm is also applicable for other absorber thicknesses.

It should be specially noted here that CIGSe solar cells have an excellent hole diffusion length up to more than 10 μm [47]. The sizes of the hemispheres investigated are within the diffusion length of holes. Further, it was experimentally demonstrated that dielectric nanostructures at the back interface are potentially able to passivate the back interface and reduce the back recombination rather than degrade CIGSe qualities or increase the interface recombination for ultrathin CIGSe cells [23, 25-28, 47]. Regarding the fabrication complexities of NPs, several

lithography technologies such as nanosphere lithography [48], substrate conformal imprint lithography [49], are able to fabricate large scale NP arrays with a high tolerance to the substrate and other environment factors. Envisaging the vast consumption of absorber materials in mass production, it is promising to employ these technologies into the fabrication of ultrathin CIGSe solar cells without a cost increase.

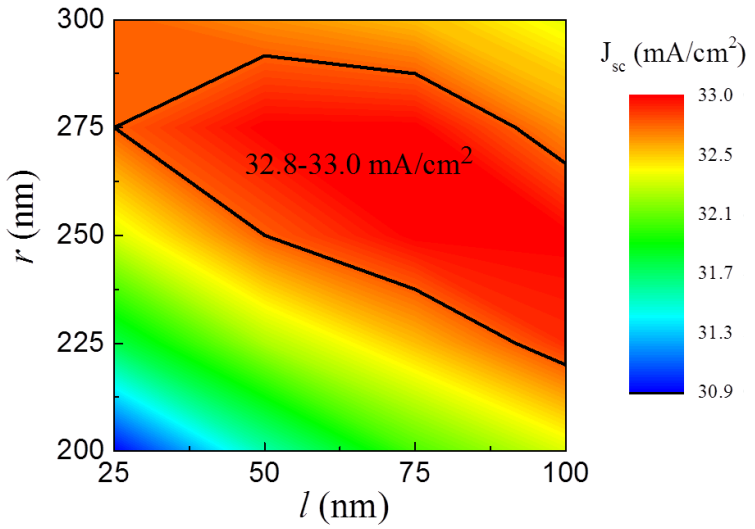


Figure 6 $J_{sc}$ contour as a function of ($r$, $l$) for CIGSe solar cells on ITO at $d_{CIGSe}$ = 400 nm under front illumination

To estimate the dependence of $Abs_{CIGSe}$ limit on $d_{CIGSe}$ for patterned cells, Figure 7 depicts $Abs_{CIGSe}$ and $T$ in terms of $J$ as a function of $d_{CIGSe}$ ranging from 300 to 500 nm. The hemisphere geometry parameter ($r$, $l$) is fixed at (275, 75) nm, which is within the optimum geometry range. $Abs_{CIGSe}$ for flat cells is also added as a reference for each $d_{CIGSe}$. The patterned cells exhibit a significant $Abs_{CIGSe}$ gain at each $d_{CIGSe}$, with a total $J_{sc}$ value from 30.4 to 34.5 mA/cm$^2$ and yielding a $T$ decrease from 5.7 to 3.2 mA/cm$^2$ as $d_{CIGSe}$ increases. For $d_{CIGSe}$ > 400 nm, around 3.0 mA/cm$^2$ gain in $Abs_{CIGSe}$ is obtained. Whereas, for $d_{CIGSe}$ < 400 nm, the $Abs_{CIGSe}$ increase is beyond 4 mA/cm$^2$ since more light interacts with NPs. The summation of $Abs_{CIGSe}$ for patterned cells and the corresponding $T$ linearly decreases with $d_{CIGSe}$. This means that even with total collection of the transmitted light via a lossless back reflector, the maximum $Abs_{CIGSe}$ would be achieved at the upper limit $d_{CIGSe}$ of 500 nm for ultrathin CIGSe solar cells.

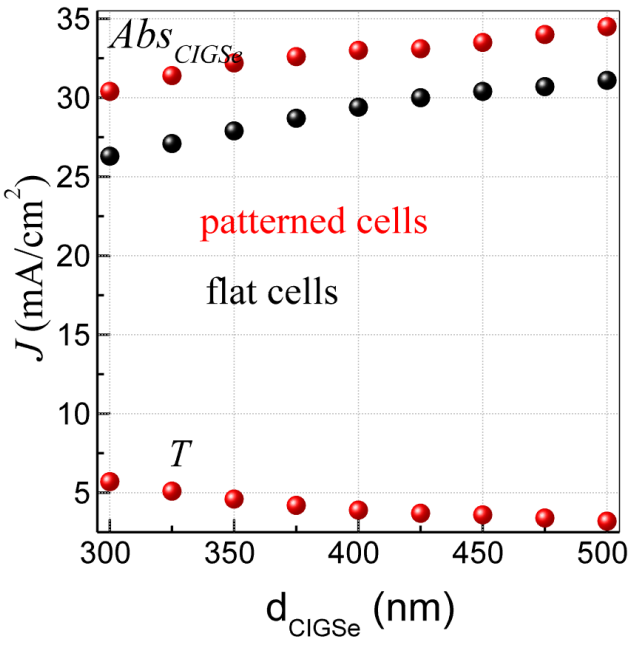


Figure 7 $Abs_{CIGSe}$ and $T$ in terms of $J$ as a function of $d_{CIGSe}$ at ($r$, $l$) = (275, 75) nm under front illumination

Figure 8 depicts $R/Abs$ (dashed lines) of patterned cells at $d_{CIGSe}$ = 500 nm after adding a Ag back reflector. As the remaining $T$ is reflected back into the cells, the $J_{sc}$ further increases up to 36.4 mA/cm$^2$, which is 1.9 mA/cm$^2$ higher than in the case without a Ag back reflector. To identify the $Abs_{CIGSe}$ gap between ultrathin cells and thick cells, $R/Abs$ of flat thick solar cells is also attached for comparison in Figure 8 (solid lines, $d_{CIGSe}$ = 2000 nm) and $Abs_{CIGSe}$ corresponds to a $J_{sc}$ of 38.7 mA/cm$^2$. This means that the ultrathin patterned cells achieve 94% $J_{sc}$ of the thick flat counterparts. The $Abs_{CIGSe}$ gap (2.3 mA/cm$^2$) lies in the infrared range, $R$ and the parasitic $Abs_{ITO}$ in the patterned cells are mainly responsible due to the still imperfect absorption.

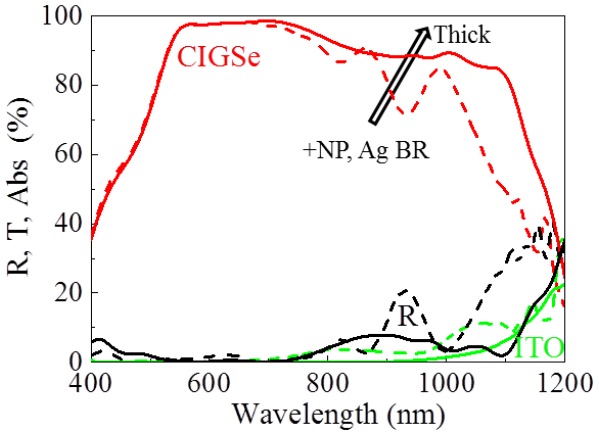

Figure 8 Optical responses (*R/Abs*) between patterned CIGSe solar cells with the addition of a Ag back reflector at the upper limit $d_{CIGSe}$ = 500 nm and (*r*, *l*) = (275, 75) nm (dashed lines) and thick flat CIGSe solar cells at $d_{CIGSe}$ = 2000 nm (solid lines)

### 5.2 Back illumination

CIGSe solar cells on a TCO back contact allow back illumination of light from the glass substrate, which is termed as a backwall structure [38]. In contrast to front illumination, the anti-reflection $MgF_2$ is not needed and a back reflector can be coated on top of the device to reflect transmitted light back into devices. Compared to the superstrate configuration with direct absorber deposition on buffer layers, the backwall structure offers the advantage of avoiding the deterioration of p-n junctions incurred by the high substrate temperature growth of CIGSe [35]. Simultaneously, ultrathin CIGSe cells are free of the carrier collection issue thick cells under back illumination are encountering, arising from the primary absorption of light close to the back of the absorber rather than at the p-n junction [38].

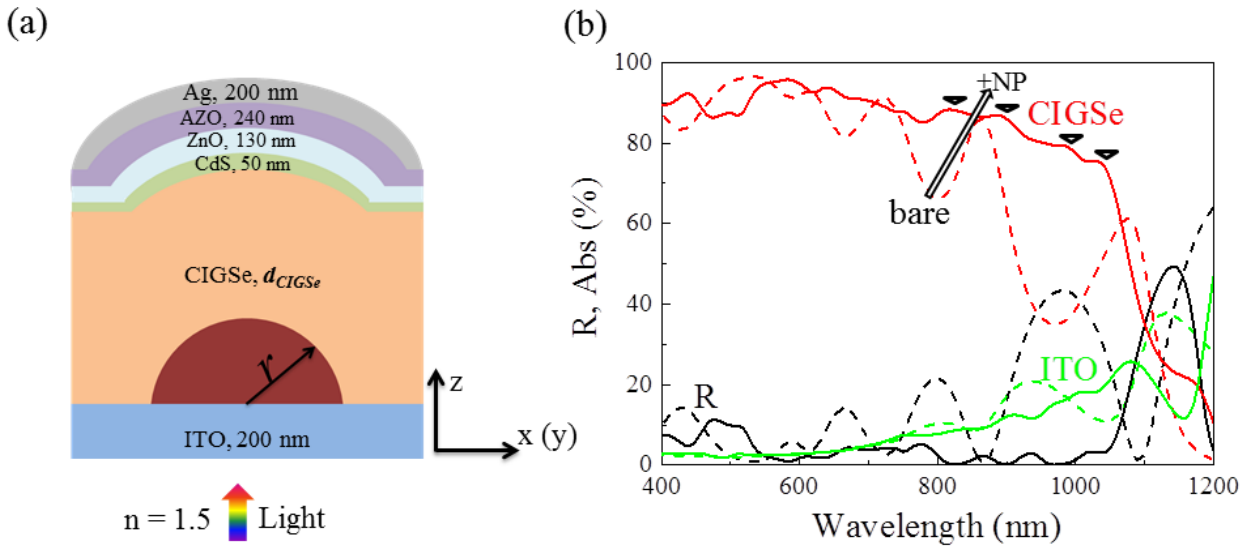


Figure 9(a) Sketch of a patterned CIGSe solar cells on ITO under back illumination, (b) corresponding optical responses (*R*/*Abs*) of flat and patterned CIGSe solar cells at $d_{CIGSe}$ = 400 nm and (*r*, *l*) = (275, 25) nm

Figure 9(a) illustrates the sketch of backwall cells with a Ag back reflector at the front side, the corresponding simulation mesh structure is shown in supporting Figure S5. To avoid the enormous computation efforts for incorporating a thick glass substrate, the approximation is assumed that the incident medium is the glass substrate. Figure 9(b) compares *R* and *Abs* between flat (dashed lines) and patterned cells (solid lines) at $d_{CIGSe}$ = 400 nm and (*r*, *l*) = (275, 25) nm under back illumination. $Abs_{CIGSe}$ in flat cells (red dashed line) exhibits pronounced Fabry–Pérot interferences and overall taper off towards longer wavelengths due to incomplete absorption. *R* (black dashed line) is becoming the main optical loss channel. The patterning flattens the Fabry–Pérot interferences of $Abs_{CIGSe}$ (red dashed to red solid lines) and overall gives a $J_{sc}$ gain as high as 4.1 mA/cm$^2$ (from 32.7 to 36.8 mA/cm$^2$). As compared in Figure 9(b), the significant $J_{sc}$ gain is originating from the constraint of *R*: after patterning, *R* (black solid line) is overall reduced to a marginal level (below 5%) with much smoother interferences.

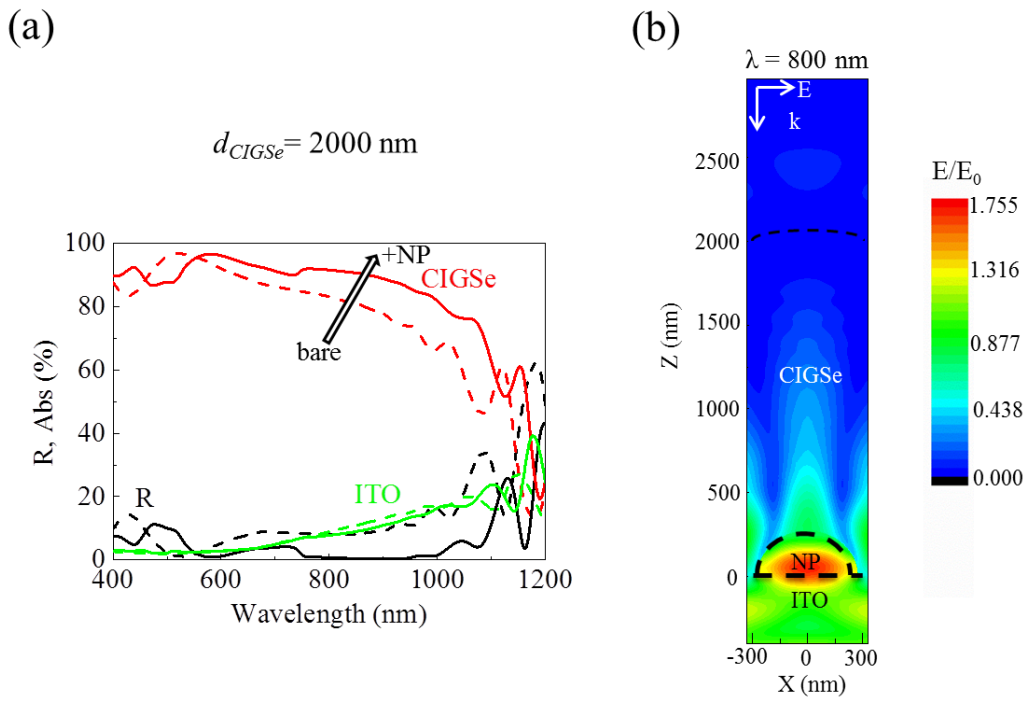


Figure 10(a) Optical responses (*R*/*Abs*) of flat and patterned CIGSe solar cells at $d_{CIGSe}$ = 2000 nm and (*r*, *l*) = (275, 25) nm under back illumination, (b) near field distribution at λ = 800 nm

As stated in the case of front illumination, dielectric NPs with sizes comparable or larger than the incident wavelengths feature dominant forward scattering ability. Back illumination can utilize this feature and the preferential direction is towards the CIGSe layer rather than towards ITO under front illumination. For a better understanding of how the dominant forward scattering contributes to the $Abs_{CIGSe}$ enhancement, we simulate cells with thick absorbers, where incident light can be completely absorbed without reaching the back contact. Figure 10(a) compares *R*/*Abs* curves between flat and patterned cells at $d_{CIGSe}$ = 2000 nm. Surprisingly, a further broadband $Abs_{CIGSe}$ enhancement (3.2 mA/cm$^2$) is observed. Similar to the ultrathin cells in Figure 9(b), *R* is greatly reduced to almost zero in the wavelength range 800-1000 nm and is mainly responsible for $Abs_{CIGSe}$ enhancement. Since the absorbers are thick enough to allow complete absorption of incident light, *R* reduction and incurred $Abs_{CIGSe}$ enhancement is then expected to be arising from improved incoupling efficiency (towards CIGSe absorbers) at ITO/CIGSe interface due to the preferential forward scattering of NPs. The preferential forward scattering behavior of dielectric NPs are typically characterized by a concentrated electric fields close to their shadow-side surface, forming a jet-like electric field distribution [45, 46]. Figure 10(b) shows the near field contour at $\lambda$ = 800 nm and we can observe that the electrical field is most concentrated within the

NP and gradually reduces in intensity as it propagates towards the CIGSe absorber, forming a jet-like field distribution (also seen at other wavelengths). However, the jet-like field distribution shown in Figure 10(b) is not observed for ultrathin CIGSe cells in Figure 9(b), this is because the light concentration phenomenon in ultrathin cells is combined with the waveguide modes (see below) and back reflecting of Ag back reflector.

Besides the dominant forward coupling efficiency at CIGSe/ITO, waveguide modes are also excited in ultrathin cells. The four $Abs_{CIGSe}$ peaks as highlighted in Figure 9(b) are also linearly red-shifting as $l$ is increasing. Therefore, the $Abs_{CIGSe}$ enhancement with the addition of NPs under back illumination is from the combined benefits of preferential forward scattering and multiple waveguide modes.

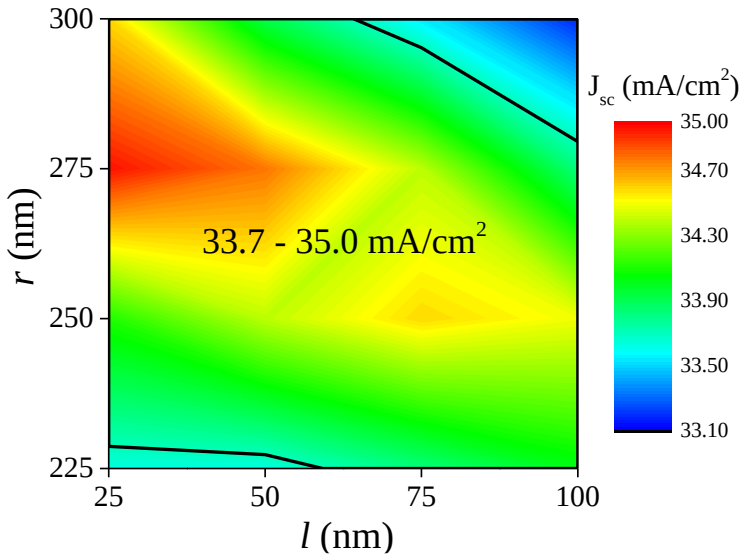


Figure 11 $J_{sc}$ contour as a function of ($r$, $l$) at $d_{CIGSe}$ = 400 nm under back illumination.

For discovering the optimum geometry range of NPs for $Abs_{CIGSe}$ enhancement under back illumination, $J_{sc}$ as a function of ($r$, $l$) for $d_{CIGSe}$ = 400 nm is mapped in Figure 11. Here, all $J_{sc}$ values calculated from the model in Figure 9(a) are calibrated with a 5% deduction for considering the loss of the single reflection at air/glass substrate. In the whole geometry range, a $Abs_{CIGSe}$ enhancement is demonstrated at least 2.1 mA/cm$^2$ and the maximum enhancement up to 3.9 mA/cm$^2$ is achievable at ($r$, $l$) = (275, 25) nm compared to flat references. Remarkably, in the most geometry ranges investigated, the patterned ultrathin cells realize a higher $Abs_{CIGSe}$ than thick flat cells at $d_{CIGSe}$ = 2000 nm (33.7 mA/cm$^2$). To identify the lower limit of $d_{CIGSe}$ for obtaining comparable $Abs_{CIGSe}$ to thick flat cells, Figure 12 depicts $Abs_{CIGSe}$ in terms of $J_{sc}$ as a

function of $d_{CIGSe}$ ranging from 300 to 500 nm under a fixed NP geometry parameter ($r$, $l$) = (275, 25) nm. Patterning gives rise to a great $Abs_{CIGSe}$ enhancement at each individual $d_{CIGSe}$. As $d_{CIGSe}$ increases, the patterned $Abs_{CIGSe}$ gradually increases and tends to saturate at 35.0 mA/cm$^2$ from $d_{CIGSe}$ = 425 nm. Remarkably, the patterned $J_{sc}$ at $d_{CIGSe}$ = 300 nm is almost equal to that of the thick flat cells at $d_{CIGSe}$ = 2000 nm, which indicates that the patterned cells under back illumination with a $d_{CIGSe}$ of only 300 nm are able to realize comparable absorption to thick flat cells.

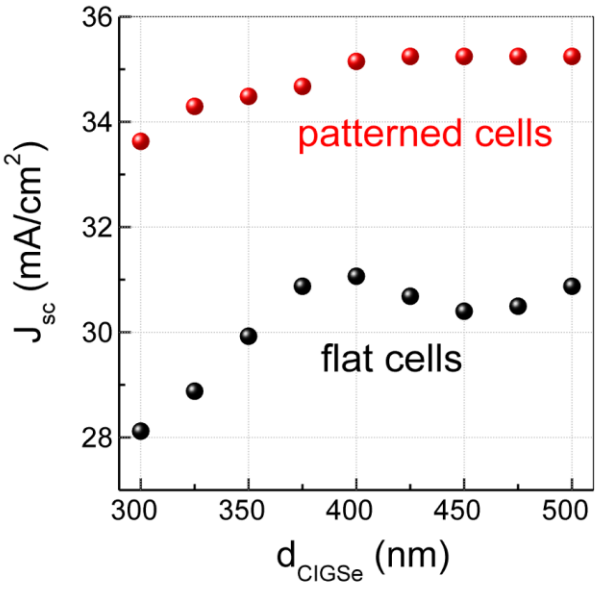


Figure 12 $Abs_{CIGSe}$ in terms of $J_{sc}$ as a function of $d_{CIGSe}$ for flat and patterned CIGSe solar cells under back illumination

Under front illumination, patterned ultrathin CIGSe solar cells reach 94% $Abs_{CIGSe}$ of their thick counterparts at the upper limit $d_{CIGSe}$ of 500 nm. In contrast, under back illumination, ultrathin cells achieve an $Abs_{CIGSe}$ equal to their thick counterparts at a $d_{CIGSe}$ of only 300 nm. However, the absolute maximum $J_{sc}$ under back illumination (35.2 mA/cm$^2$, Figure 12) is lower than the maximum value under front illumination (36.8 mA/cm$^2$, Figure 8). Reviewing Figure 9(b), $Abs_{ITO}$ is the main factor suppressing a greater maximum $Abs_{CIGSe}$ under back illumination. The parasitic $Abs_{ITO}$ is mainly stemming from the free carriers necessary for a good conductivity as a back contact. This indicates that the advantage of back illumination for achieving the maximum $Abs_{CIGSe}$ at a lower $d_{CIGSe}$ is dissipated due to a lower maximum $Abs_{CIGSe}$ compared to front illumination. High-mobility TCOs (e.g. H:$In_2O_3$) feature higher carrier mobility and less carrier

concentration, which guarantees good conductivity without increasing absorption ability [32, 50]. Applying them to replace ITO may be a promising option to further reduce the parasitic absorption in the back contact and utilize the advantage of back illumination.

Additionally, in module configuration, 1) $MgF_2$ will be replaced by encapsulation EVA and glass substrate with an index around 1.5, 2) a much thicker AZO (around 1000 nm) will be applied for lateral transport of electrons under front illuminated cells. This will respectively give rise to an increased $R$ and parasitic $Abs_{top}$, leading to a significantly reduced $J_{sc}$ compared to the lab-scale cells shown in this work. Whereas under back illumination, due to the very good conductivity of the Ag back reflector, AZO is even not necessary. Even with a dielectric back reflector (*e.g.* $TiO_2$ paste), absorption in AZO/ZnO/CdS with a thicker AZO layer will be still negligible since most light is first absorbed by the patterned CIGSe absorbers. Therefore, the maximum $J_{sc}$ is expected to be much greater under back illumination than under front illumination in module configuration. To simply quantify this, Figure 13 shows the simulated *Abs* of patterned ultrathin solar cells in module configuration with a 1000 nm thick AZO under two different illumination directions. For calculation simplicity, light is assumed incident from glass substrate in both illumination cases. As expected, the parasitic absorption in AZO under front illumination is quite severe, which causes a much reduced $Abs_{CIGSe}$ with respect to the corresponding lab-scale cells. In contrast, under back illumination, $Abs_{CIGSe}$ can reach 33.5 mA/cm$^2$, which is 3.6 mA/cm$^2$ higher than the value under front illumination. This indicates that the back illuminated hemisphere patterned ultrathin CIGSe solar cells will be a promising structure for high efficiencies in module production.

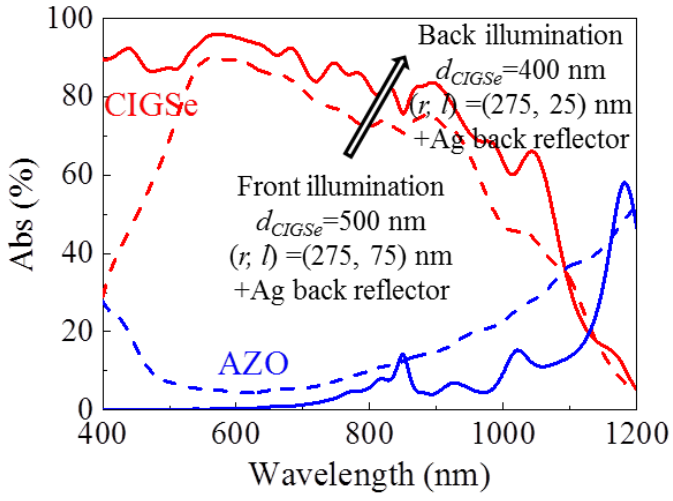

Figure 13 *Abs* curves of patterned ultrathin CIGSe solar cells with a 1000 nm thick AZO and a Ag back reflector under both front and back illuminations

# 6. Conclusion

In this work, we extensively examined light trapping effects of dielectric NPs in ultrathin CIGSe solar cells from three aspects: interface locations of NPs, back contacts and illumination configurations. The conclusions are as follows:

1) The parasitic absorption in Mo is the main optical loss for flat ultrathin CIGSe solar cells and is also the main constraining factor for achieving a significant $Abs_{CIGSe}$ enhancement in NP-patterned ultrathin cells. The TCO/glass/back reflector back contact structure (ITO/glass/Ag in this work), exhibiting much less parasitic absorption and excellent back-reflecting ability, is recommended to replace the conventional Mo for a higher $Abs_{CIGSe}$.

2) NPs are favoured to be directly placed at the interface of CIGSe/back contact. This allows light trapping effects of NPs being utilized to the greatest extent by the CIGSe absorbers rather than being attenuated by other non-active layers.

3) Under front illumination, the hemisphere ($n$ =1.5) patterned ultrathin CIGSe solar cells on ITO show a significant $Abs_{CIGSe}$ enhancement, which is due to the joint effects of waveguides modes and back scattering of NPs. The broadband improvement of back scattering and especially the multiplicity of waveguide modes determine the broadness of the geometry range of hemisphere arrays for a maximum $Abs_{CIGSe}$. In conjunction with a Ag back reflector, the maximum $J_{sc}$ reaches 36.4 mA/cm$^2$ at the upper $d_{CIGSe}$ = 500 nm, 94% of that of their thick flat counterparts.

4) The ITO substrate also allows back illumination and utilization of a back reflector in the front. The hemispherical NPs contributes to a broadband $Abs_{CIGSe}$ gain via their preferential forward scattering and waveguide modes, which reduces $R$ to minimum and traps light within CIGSe absorbers. Consequently, the patterned CIGSe solar cells are able to reach comparable $Abs_{CIGSe}$ to their thick cells at a $d_{CIGSe}$ of only 300 nm, and the maximum $J_{sc}$ saturates at a value of 35.2 mA/cm$^2$ at $d_{CIGSe}$ = 425 nm.

5) For lab-scale cell configurations, in contrast to front illumination, the advantage of back illumination of achieving its maximum $J_{sc}$ at a low $d_{CIGSe}$ is shadowed because of a relatively lower maximum $J_{sc}$ due to the strong parasitic absorption in ITO back contact. However, in module configuration with a much thicker AZO, the patterned cells are less affected by the heavy absorption in AZO under back illumination than under front illumination and thus exhibit a much higher $Abs_{CIGSe}$. This suggests that patterned ultrathin CIGSe solar cells on TCO substrate under back illumination will be a promising structure for high efficiencies in industrial module production.

# Acknowledgements

The authors acknowledge the funding from the Helmholtz-Association for Young Investigator groups within the Initiative and Networking fund (VH-NG-928). The results were obtained with the assistance of the Berlin Joint Lab for Optical Simulations for Energy Research (BerOSE) of Helmholtz-Zentrum Berlin für Materialien und Energie, Zuse Institute Berlin, and Freie Universität Berlin.

# References

1. https://www.zsw-bw.de/en/newsroom/news/news-detail/news/detail/News/zsw-sets-new-world-record-for-thin-film-solar-cells.html, 2016.
2. CIGS community, White paper for CIGS thin film solar cell technology, 2016.
3. Tao, C.S., et al., 2011. Natural Resource Limitations to Terawatt-Scale Solar Cells. Sol. Energy Mater. Sol. Cells 95(12), 3176–3180.
4. Fthenakis, V., 2012. Sustainability of photovoltaics: The case for thin-film solar cells. Renew. Sustainable Energy Rev. 13(9), 2746-2750.
5. Gloeckler, M., Sites, J.R., 2005. Potential of submicrometer thickness Cu(In,Ga)$Se_2$ solar cells. J. Appl. Phys. 98(10),103703.
6. Jehl, Z., Erfurth, F., Naghavi, N., Lombez, L., Gerard, I., Bouttemy, M., Tran-Van, P., Etcheberry, A., Voorwinden, G., Dimmler, B., Wischmann, W., Powalla, M., Guillemoles, J. F., Lincot, D. 2011.Thinning of CIGS solar cells: Part II: Cell characterizations. Thin Solid Films 519(21), 7212–7215.
7. Lundberg, O., Bodegärd, M., Malmström, J., Stolt, L., 2003. Influence of the Cu(In,Ga)$Se_2$ thickness and Ga grading on solar cell performance. Prog. Photovoltaics Res. Appl. 11(2), 77–88.
8. Yin, G., Brackmann, V., Hoffmann, V., Schmid, M., 2014. Enhanced performance of ultra-thin Cu(In,Ga)$Se_2$ solar cells deposited at low process temperature. Sol. Energy Mater. Sol. Cells 132, 142–147.
9. Catchpole, K. R., Polman, A., 2008. Plasmonic solar cells Opt. Express 16(26), 21793–21800.

10. Spinelli, P., Polman, A., 2012. Prospects of near-field plasmonic absorption enhancement in semiconductor materials using embedded Ag nanoparticles. Opt. Express 20(S5), A641.
11. Tan, H., Santbergen, R., Smets, A. H., Zeman, M., 2012. Plasmonic light trapping in thin-film silicon solar cells with improved self-assembled silver nanoparticles. Nano Lett. 12(8), 4070–4076.
12. Atwater, H.A., Polman, A., 2010. Plasmonics for improved photovoltaic devices. Nat. Mater. 9(3), 205–213.
13. Ferry, V.E., Sweatlock, L.A., Pacifici, D., Atwater, H.A., 2008. Plasmonic nanostructure design for efficient light coupling into solar cells. Nano Lett. 8(12), 4391–4397.
14. Ferry, V.E., Verschuuren, M.A., Li, H.B.T., Verhagen, E., Walters, R.J., Schropp, R.E.I., Atwater, H.A., Polman, A., 2010. Light trapping in ultrathin plasmonic solar cells. Opt. Express 18(S2), A237–A245.
15. Schmid, M., Andrae, P., Manley, P., 2014. Plasmonic and photonic scattering and near fields of nanoparticles. Nanoscale Res. Lett. 9(1), 50.
16. Yin, G., Steigert, A., Andrae, P., Goebelt, M., Latzel, M., Manley, P., Lauermann, I., Christiansen, S., Schmid, M., 2015. Integration of plasmonic Ag nanoparticles as a back reflector in ultra-thin Cu(In,Ga)$Se_2$ solar cells. Appl. Surf. Sci. 355, 800–804.
17. Spinelli, P., Verschuuren, M, Polman, A., 2012. Broadband omnidirectional antireflection coating based on subwavelength surface Mie resonators. Nat. Commun. 3, 692.
18. Brongersma, M.L., Cui, Y., Fan, S., 2014. Light management for photovoltaics using high-index nanostructures. Nat. Mater. 13(5), 451–460.
19. Mann, S.A., Grote, R.R., Osgood, R.M., Schuller, J.A., 2011. Dielectric particle and void resonators for thin film solar cell textures. Opt. express 19 (25), 25729–25740.
20. Wang, E-C., Mokkapati, S., White, T., Soderstrom, T., Varlamov, S., Catchpole, K., 2014. Light trapping with titanium dioxide diffraction gratings fabricated by nanoimprinting. Prog. Photovoltaics Res. Appl. 22, 587-592.
21. Hoex, B., Schmidt, J., Bock, R., Altermatt, P.P., Sanden, M.C.M., Kessels, W.M.M., 2007. Excellent passivation of highly doped p-type Si surfaces by the negative-charge-dielectric $Al_2O_3$. Appl. Phy. Lett. 91(11), 112107.
22. Moors, M., Baert, K., Caremans, T., Duerinckx, F., Cacciato, A., Szlufcik, J., 2012. Industrial PERL-type solar cells exceeding 19% with screen-printed contacts and homogeneous emitter. Sol. Energy Mater. Sol. Cells 106, 84–88.
23. Vermang, B., Fjällström, V., Pettersson, J., Salomé, P., Edoff, M., 2013. Development of rear surface passivated Cu(In,Ga)$Se_2$ thin film solar cells with nano-sized local rear point contacts. Sol. Energy Mater. Sol. Cells 117, 505–511.
24. Yin, G., Manley, P., Schmid, M., 2016. Light absorption enhancement for ultra-thin Cu($In_{1-x}Gax$)$Se_2$ solar cells using closely packed 2-D $SiO_2$ nanosphere arrays. Sol. Energy Mater. Sol. Cells 153,124–130.
25. Lare C., Van, Yin, G., Polman, A., Schmid, M., 2015. Light Coupling and Trapping in Ultrathin Cu (In,Ga)$Se_2$ Solar Cells Using Dielectric Scattering Patterns. ACS Nano 9(10), 9603–9613.
26. Yin, G., Knight, M.W., Lare C., Van, Garcia, M.M.S., Polman, A., Schmid, M., 2016. Optoelectronic Enhancement of Ultrathin $CuIn_{1-x}Ga_xSe_2$ Solar Cells by Nanophotonic Contacts. Adv. Opt. Mater. 5(5), 1600637.
27. Yin, G., Song, M., Duan, S., Manley, P., Greiner, D., Kaufmann, C.A., Schmid, M., 2016. Well-Controlled Dielectric Nanomeshes by Colloidal Nanosphere Lithography for

Optoelectronic Enhancement of Ultrathin Cu(In,Ga)$Se_2$ Solar Cells. ACS Appl. Mater. Interfaces 8(46), 9603-9613.
28. Salome, P. M. P., Vermang, B., Ribeiro-Andrade, R., Teixeira, J. P., Cunha, J. M. V., Mendes, M. J., Haque, S., Borme, J., Aguas, H., Fortunato, E., Martins, R., Gonzalez, J. C., Leitao, J. P., Fernandes, P. A., Edoff, M., Sadewasser, S., 2017. Passivation of Interfaces In Thin Film Solar Cells: Understanding the Effects of a Nanostructured Rear Point Contact Layer. Adv Mater. Interfaces 1701101.
29. Yin, G., Merschjann, C., Schmid, M., 2013. The effect of surface roughness on the determination of optical constants of $CuInSe_2$ and $CuGaSe_2$ thin films. J. Appl. Phys. 113(21), 213510.
30. https://www.helmholtz-berlin.de/forschung/oe/ee/nanooptix/refdex/index_en.html.
31. http://www.jcmwave.com/.
32. Onwudinanti, C., Vismara, R., Isabella, O., Grenet, L., Emieux, F., Zeman, M., 2016. Advanced light management based on periodic textures for Cu(In,Ga)$Se_2$ thin-film solar cells. Opt. Express 24(6), A693.
33. Krc, J., Sever, M., Campa, A., Lokar, Z., Lipovsek, B., Topič, M., 2016. Optical confinement in chalcopyrite based solar cells. Thin Solid Films in press. http://dx.doi.org/10.1016/j.tsf.2016.08.056
34. Li-kao, Z.J., Naghavi, N., Erfurth, F., Guillemoles, J.F., Gérard, I., Etcheberry, A., Pelouard, J.L., Collin, S., Voorwinden, G., Lincot, D., 2012. Towards ultrathin copper indium gallium diselenide solar cells : proof of concept study by chemical etching and gold back contact engineering. Prog. Photovolt.: Res. Appl. 20, 582–587.
35. Young, D.L., Abushama, J., Noufi, R., Li, X., Keane, J., Gessert, T.A., Ward, J.S., Contreras, M., Coutts, T.J.A, 2002. New Thin-Film $CuGaSe_2$/Cu (In,Ga)$Se_2$ Bifacial, Tandem Solar Cell with Both Junctions Formed Simultaneously Preprint. *Record of the Twenty-Ninth IEEE Photovoltaic Specialists Conference* 608–611.
36. Nakada, T., 2005. Microstructural and diffusion properties of CIGS thin film solar cells fabricated using transparent conducting oxide back contacts. Thin Solid Films 480-481, 419–425.
37. Nakada, T., Hirabayashi, Y., Tokado, T., Ohmori, D., Mise, T., 2004. Novel device structure for Cu(In,Ga)$Se_2$ thin film solar cells using transparent conducting oxide back and front contacts. Sol. Energy 77(6), 739–747.
38. Larsen, J.K., Simchi, H., Xin, P., Kim, K., Shafarman, W.N., 2014. Backwall superstrate configuration for ultrathin Cu(In,Ga)$Se_2$ solar cells. Appl. Phys. Lett. 104(3), 033901.
39. Simchi, H., McCandless, B.E., Meng, T., Shafarman, W.N., 2014. Structure and interface chemistry of $MoO_3$ back contacts in Cu(In,Ga)$Se_2$ thin film solar cells. J. Appl. Phy. 115(3), 033514.
40. Dahan, N., Jehl, Z., Hildebrandt, T., Greffet, J.J., Guillemoles, J.F., Lincot, D., Naghavi, N. Optical approaches to improve the photocurrent generation in Cu(In,Ga)$Se_2$ solar cells with absorber thicknesses down to 0.5 μm. J. Appl. Phy. 112(9), 0–7.
41. Sanchez-Sobrado, O., Mendes, M. J., Haque, S., Mateus, T., Araujo, A., Aguas, H., Fortunato, E., Martins, R., 2017. Colloidal-lithographed $TiO_2$ Photonic Nanostructures for Solar Cell Light Trapping. J. Mater. Chem. C. 5, 6852-6861.
42. Sever, M., Lipovsek, B., Krc, J., Campa, A., Plaza, G.S., Haug, F., Duchamp, M., Soppe, W., Topic, M., 2013. Combinedmodel of non-conformal layer growth for accurate optical simulation of thin film silicon solar cells. Sol. Energy Mater. Sol. Cells 119, 59-66.

43. Mokkapati, S., Catchpole, K.R., 2012. Nanophotonic light trapping in solar cells. J. Appl. Phy. 112(10), 101101.
44. Heifetz, A., Kong, S.-C., Sahakian, A.V., Taflove, A., Backman, V., 2009. Photonic Nanojets. J. Comput. Theor. Nanosci. 6(9), 1979–1992.
45. Chen, Z., Taflove, A., Backman, V., 2004. Photonic nanojet enhancement of backscattering of light by nanoparticles: a potential novel visible-light ultramicroscopy technique. Opt. Express 12(7),1214–1220.
46. Itagi, A.V., Challener, W.A., 2005. Optics of photonic nanojets. J. Opt. Soc. Am. A Opt. Image Sci. 22(12), 2847–2858.
47. Casper, P., Hünig, R., Gomard, G., Kiowski, O., Reitz, C., Lemmer, U., Powalla, M., Hetterich, M., 2016. Optoelectrical Improvement of Ultra-Thin Cu(In,Ga)$Se_2$ Solar Cells through Microstructured $MgF_2$ and $Al_2O_3$ Back Passivation Layer. Phys. Status Solidi RRL 10(5), 376-380.
48. Kandulski W., 2007. Shadow Nanosphere Lithography. Dissertation, Bonn.
49. Verschuuren M.A., 2010. Substrate Conformal Imprint Lithography for Nanophotonics. Dissertation, Utrecht.
50. Yin, G., Steigert, A., Manley, P., Klenk, R., Schmid, M., 2015. Enhanced absorption in tandem solar cells by applying hydrogenated $In_2O_3$ as electrode. Appl. Phys. Lett. 107(21), 1–5.